ORIGINAL ARTICLE

Assessing Dihydrotestosterone-Induced Skin Alterations in C57BL/6 Mice: Implications for Androgenetic Alopecia through High-Resolution Ultrasound Imaging

Sadegh Shurche[1], Manijhe Mokhtari-Dizaji[1*], Mansoureh Movahedin[2], Mohammad Ali Nilforoshzade[3], Ehsan Taghiabadi[3]

[1] *Department of Medical Physics, Faculty of Medical Sciences, Tarbiat Modares University, Tehran, Iran*

[2] *Department of Anatomical Sciences, Faculty of Medical Sciences, Tarbiat Modares University, Tehran, Iran*

[3] *Skin and Stem Cells Research Center, Tehran University of Medical Sciences, Tehran, Iran*

*Corresponding Author: Manijhe Mokhtari-Dizaji
Email: mokhtarm@modares.ac.ir

Received: 03 February 2025 / Accepted: 08 April 2025

Abstract

Purpose: There are different types of hair loss known as alopecia. Various methods for treating Androgenetic Alopecia (AGA) are being investigated in the preclinical stage using C57BL/6 mice affected by this condition.

The purpose of the study was to evaluate the effects of Dihydrotestosterone (DHT) on the skin layers of male C57BL/6 mice, simulating a model of AGA using high-resolution ultrasound imaging.

Materials and Methods: Seven-week-old male C57BL/6 mice were selected for the study. To induce AGA, three of the mice received intraperitoneal injections of DHT at a dosage of 1 mg per day for five consecutive days, a known method for provoking hair loss via androgenic pathways. High-resolution ultrasound imaging at 40 and 75 MHz frequencies allowed detailed observation of skin layer changes due to DHT administration. Shear modulus and Young modulus were extracted using dynamic loading throughout ultrasonography with a 40 MHz frequency. Both control and AGA-affected groups were evaluated through structural imaging and were compared with histopathological results. Tissues were stained with Hematoxylin-Eosin (H&E) and Trichrome Mason.

Results: Ultrasound imaging revealed that the epidermis thickness was 0.22±0.01 mm in the control group compared to 0.31±0.02 mm in the AGA group at 40 MHz. At 75 MHz, these measurements were 0.10±0.05 mm for the control group and 0.20±0.01 mm for the AGA group. The dermis thickness measurements showed 0.30±0.02 mm in the control group and 0.70±0.04 mm in the AGA group at 40 MHz, while at 75 MHz, the thicknesses were 0.40±0.02 mm for the control group and 0.70±0.04 mm for the AGA group. H&E staining results aligned with these ultrasound findings, confirming increased epidermal and dermal thicknesses in the AGA group. Elasticity metrics indicated a shear modulus of 1.19±0.60 kPa for the control group and 6.70±0.33 kPa for the AGA group, while Young modulus demonstrated values of 6.47±0.32 kPa for the control group and 22.69±1.13 kPa for the AGA group. Further corroboration of altered tissue elasticity was provided by Trichrome staining, indicating significant changes in skin structure.

Conclusion: The administration of DHT in the C57BL/6 mice model leads to notable structural changes in skin layers, evidenced by an increased thickness of both the epidermis and dermis, along with diminished mechanical properties of skin elasticity.

Keywords: High-Resolution Ultrasound Imaging; Androgenetic Alopecia; Skin Biomechanics; Dihydrotestosterone; Elastic Modulus.

DOI:

1. Introduction

Alopecia, commonly known as hair loss, is a significant dermatological condition that affects millions of people worldwide. One of its most common forms is Androgenetic Alopecia (AGA), which impacts nearly 50% of Caucasian men by age 50 and a substantial number of women throughout their lives [1-3]. AGA is characterized by progressive hair thinning, primarily driven by androgenic activity, particularly the effects of Dihydrotestosterone (DHT) on susceptible hair follicles. DHT is known to shorten the anagen phase of the hair cycle and promote follicular miniaturization, both of which play crucial roles in the development of AGA [4, 5]. Despite being widespread, the underlying mechanisms of AGA are only partially understood, leading to ongoing research into its genetic and hormonal influences. Animal models, especially the C57BL/6 mouse strain, have proven invaluable in this exploration. Although this strain naturally lacks significant scalp hair, it provides a robust platform for studying hair follicle biology due to its well-characterized response to androgenic stimuli, such as DHT [6, 7]. By administering DHT to these mice, researchers can replicate the conditions of AGA, allowing for preclinical investigations into therapeutic approaches and the mechanisms of the disease [8, 9]. However, most previous studies have utilized traditional imaging methods such as histopathology, clinical photography, and various optical imaging techniques, which, while providing data on thickness and certain microscopic changes, have generally been unable to offer precise quantitative measurements of the skin's biomechanical properties. Various diagnostic techniques, including photography, dermoscopy, reflective confocal microscopy, Optical Coherence Tomography (OCT), and high-frequency ultrasound, can assist in identifying skin tissue disorders [10-12]. Advanced imaging techniques such as OCT and confocal microscopy have been capable of capturing high-resolution details of superficial and structural features [13]. However, they face limitations in penetrating deeply into the skin layers and in accurately assessing biomechanical properties (such as shear modulus and Young modulus) [14]. In this regard, studies using non-invasive methods for evaluating skin strength and elasticity have generally encountered limitations related to numerical precision and data reproducibility [13]. High-resolution ultrasound imaging offers a non-invasive, radiation-free method for real-time diagnostic assessments. Its growing application in skin tissue analysis enables the examination of both healthy and diseased skin while also tracking changes within the skin's layers [15-17]. The skin, being the outermost soft tissue of the body, is composed of multiple layers. High-frequency ultrasound imaging allows for the capture of detailed images of these layers [18]. The primary component is the epidermis, the outermost layer made of keratinocytes. Despite its thin structure, ranging between 0.02 and 0.15 mm, it serves as a strong barrier against various pathogens [19]. This layer also contains proliferative cells that actively divide and move upwards to replace the cells in the outer layers [20]. Beneath the epidermis lies the dermis, the thickest layer of skin, measuring between 0.6 and 3.0 mm in humans. The dermis plays a crucial role in regulating body temperature and supplying blood to the epidermis [21]. This study seeks to expand upon existing knowledge by leveraging high-resolution ultrasound to observe the effects of DHT on the skin layers of male C57BL/6 mice. By closely monitoring alterations in both skin thickness and elasticity, we aim to elucidate the structural changes underlying AGA.

2. Materials and Methods

2.1. Ethics Statement

The experiments took place at the Tarbiat Modares University Laboratory in Tehran, Iran. Every effort was made to reduce animal suffering, and the study adhered to the guidelines approved by the "Tarbiat Modares University Ethical Committee for Animal Research" (Code: IR.MODARES.AEC.1402.024).

2.2. Animals

7-week-old male C57BL/6 mice were used to create the androgenetic alopecia model. They were kept under standard animal house conditions (22–23°C, 12–12 light-dark cycle, tap water, and standard laboratory diet). All experiments were performed according to the ARRIVE guidelines [22]. During the AGA induction and imaging session, the mice were

anesthetized [23] with a mix of Ketamine and Xylazine.

2.3. AGA Model on Male C57BL/6 Mice

DHT powder (Sigma-Aldrich Inc., USA) was dissolved in corn oil (Sigma-Aldrich Inc., USA) and injected intraperitoneally into 7-week-old male mice to create the androgenetic alopecia model. The injections were administered for 5 consecutive days. The hair of the mice was shaved on the fifth day of injection, and the hair growth process was examined.

2.4. Tracking the Growth Process of Mice's Hair

Photographs of mice in the control group and those with androgenetic alopecia were taken on the days before and after shaving (Figure 1). The growth cycle of mouse hair is 21 days, which is why the growth process of mouse hair was investigated until day 24 after shaving. Because the injection of DHT causes changes in the weight of mice, hair thickness (by optical microscope), and length (by digital ruler) of mice; therefore, these factors will be investigated in two control groups and those under drug injection.

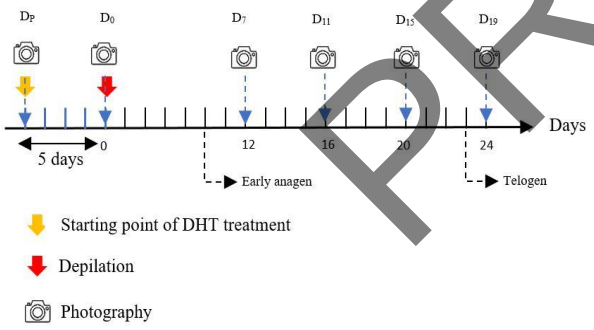

Figure 1. Creating an AGA model in male C57BL/6 mice using DHT injection. The injection was administered intraperitoneally for 5 consecutive days, and after this period, the hair of the mice was shaved. The days on which the photographs were taken are displayed on the axis (D_P (starting point of DHT treatment), D_0 (epilation day), D_7 (7^{th} day), D_{11}(11^{th} day), D_{15}(15^{th} day), and D_{19}(19^{th} day))

2.5. High-Resolution Ultrasound Imaging

Ultrasound imaging of the skin layers was performed utilizing high-frequency transducers at 40 MHz (Ultrasonix Company, Richmond, Canada; with a resolution of 0.01 mm in both longitudinal and transverse directions) and 75 MHz (DUB skin scanner, TPM company, UK, London, with a maximum axial resolution of 0.021 mm). The 75 MHz transducer offers exceptionally high-resolution images due to its higher frequency, enabling researchers to observe the various layers of skin, such as the epidermis and dermis, with enhanced precision. This facilitates more accurate measurement of tissue changes and thin skin layers. In contrast, the 40 MHz transducer allows for greater penetration depth, essential for evaluating deeper skin structures. This trade-off between resolution and penetration depth allows researchers to study different skin layers according to their depth, providing a thorough understanding of skin morphology. B-mode images from the 40 MHz ultrasound system (depth: 1 cm, gain: 60%) were obtained from the left, right, and center of the skin. To reduce error, the thickness of the layers in each image was measured five times. The dimensions of the skin tissue layers, including the dermis and epidermis, were extracted using ImageJ software (a Java-based image processing program, version 1.52 for Windows). For the 75 MHz frequency imaging, a scan of the skin was conducted, and the thickness, density, and number of pixels of the skin texture were automatically assessed.

2.6. Elasticity Measurements (Shear Modulus and Young Modulus)

To assess skin elasticity, the method described by Estaji *et al.* [24] was employed. This procedure involves analyzing the mechanical behavior of skin under dermatological conditions using a force gauge device (Lutron Co., Taipei, Taiwan, 0.01 N), which is attached to the probe. This setup allows for monitoring and controlling the applied stress while recording ultrasound images. Initially, the probe with an impedance-matching gel was placed on the skin, and images were captured with no applied force, followed by the application of a 0.12 N force. As axial stress was applied to the skin, ultrasound images were continuously captured at 30 frames per second in AVI format. Under this force, the tissue is assumed to behave linearly per Hooke's law. The sequential images, in AVI format, were then transferred to a computer where a MATLAB (ver. 7.10.0.499, Math Works Inc.) script converted them into BMP format frames.

The core methodology involves an algorithm that utilizes image gradients to measure the instantaneous displacement of skin layers. Initially, longitudinal markers are placed in the axial direction in the first image to define a search range, which helps track displacement over time accurately. The boundaries between the epidermis and dermis are manually marked to improve measurement precision. The algorithm processes each frame to determine the coordinates of the epidermal and dermal layers, allowing for the calculation of instantaneous thickness changes by comparing coordinate differences across frames. This sequential analysis enables the determination of thickness variations in response to applied stress (ΔP). To quantify the mechanical properties, Young's modulus (E) is calculated using the formula (Equation 1):

$$Young\ modulus = \frac{\Delta P}{\frac{\Delta y}{y_0}} \quad (1)$$

Where Δy represents the change in thickness and y_0 is the initial thickness of the skin layer. This calculation is pivotal in understanding the material properties under dynamic conditions.

For longitudinal strain assessment, a block-matching algorithm is employed. This involves selecting a reference block from the initial frame and locating its corresponding block in subsequent frames, maintaining a constant block size throughout the analysis. Two blocks with dimensions 53×42 pixels are strategically placed on the dermal layer, with a defined separation distance (e.g., 10 pixels) to ensure reliable displacement measurements. The program analyzes sequential frames to extract maximum (x_0) and minimum distances (x_1) between the two blocks under applied stress (as 0.12 N). Shear strain calculated from the relationship (Equation 2):

$$Shear\ strain = \frac{\Delta x}{x_0} \quad (2)$$

Where Δx denotes the change in distance between the blocks. Following multiple strain measurements in the x-direction, the shear modulus (G) is determined using:

For longitudinal strain assessment, a block-matching algorithm is employed. This involves selecting a reference block from the initial frame and locating its corresponding block in subsequent frames, maintaining a constant block size throughout the analysis. Two blocks with dimensions 53×42 pixels are strategically placed on the dermal layer, with a defined separation distance (e.g., 10 pixels) to ensure reliable displacement measurements. The program analyzes sequential frames to extract maximum (x_0) and minimum distances (x_1) between the two blocks under applied stress (noted as 0.12 N). Shear modulus is calculated from the relationship (Equation 3):

$$Shear\ modulus = \frac{\frac{\Delta P}{\Delta x}}{x_0} \quad (3)$$

2.7. Histological Examinations

In this study, skin samples from C57BL/6 mice were immediately fixed in 10% formalin (or 4% phosphate-buffered formalin) for at least 24 hours. After which the samples were processed by sequential dehydration through ethanol series (70%, 95%, and 100%) and cleared in xylene to remove paraffin; subsequently, 4–5 µm thick sections were cut from the paraffin blocks using a microtome and mounted onto adhesive slides, which were then hydrated in distilled water, stained with hematoxylin for 5 to 10 minutes, and rinsed under running water to remove excess dye. The slides were briefly immersed in a differentiating solution for a few seconds to one minute to eliminate over-staining, followed by a 1 to 2 minute exposure to a bluing agent (such as 0.2% ammonia water or an equivalent) to develop the desired blue hue in the nuclei; thereafter, the sections were counterstained with eosin Y for 1 to 3 minutes to highlight the cytoplasmic components, rinsed again to remove any residual stain, then dehydrated once more through ethanol series (70%, 95%, and 100%), cleared with xylene, and finally mounted with a drop of a clear mounting medium (e.g., DPX or Permount) under a cover slip to preserve the integrity of the stained tissue for microscopic examination. They were also stained with Masson's trichrome for light microscopy and digital image acquisition (Olympus, CX33, Hamburg, Germany, magnification 100).

2.8. Statistical Analysis

Statistical analysis was performed using SPSS 22.0 software (SPSS, Inc., Chicago, IL, USA). Results are

reported as mean ± standard deviation (SD). Each experiment was repeated at least three times. We used an independent t-test to check the significant difference.

3. Results

3.1. AGA model on Male C57BL/6 Mice

Photographs of mice in the control group and those with AGA were taken in the days before and after shaving, as shown in Figure 1, and the images are presented in Figure 2A. A delay in hair growth can be seen in mice injected with DHT. Weight control of the mice was done before shaving the hair of the mice, and also on the 7th, 11th, 15th, and 19th days after shaving the hair of the mice. Weight gain in mice with AGA is less than in the healthy group. The hair diameter and length of the mice in two groups of control and affected by AGA, were measured nineteen days after shaving andare shown in Figure 2B and 2C.

The image of H&E staining of the skin of control and AGA mice, nineteen days after shaving, is shown in Figure 3. As can be seen, the number of hair follicles in the diseased mice has decreased, and the thickness of different skin layers has increased in the diseased mice compared to the control mice. Melanin around hair follicles is reduced in mice with AGA. Masson's trichrome image of the skin of control and AGA mice, nineteen days after shaving, is shown in Figure 4. As can be seen, there is disruption in the skin layers of AGA mice compared to control mice. The number of hair follicles in healthy mice was 101±5, while the number of hair follicles in mice with AGA was 45±2 (Figure 3C). The average diameter of hair follicles in mice with AGA was 16.04±0.80 micrometers, while the average diameter of hair follicles in healthy mice was 31.62±1.55 micrometers (Figure 3D). The independent t-test showed a significant difference between the number of hairs in the control group and the alopecia group ($P<0.05$).

3.2. High-Resolution Ultrasound Imaging

High-frequency ultrasound images are shown by the 40 MHz and 75 MHz probes in Figure 4. As can be seen in these images, the epidermis, dermis, and subcutaneous layers are clearly visible in both images.

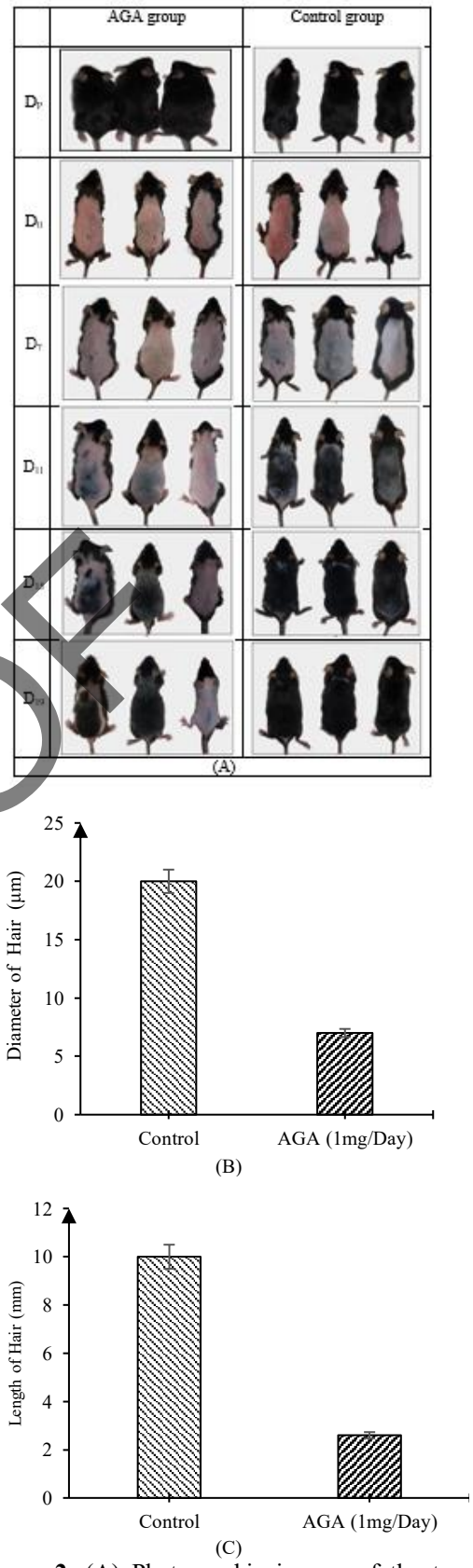

Figure 2. (A) Photographic images of the two control and Androgenetic alopecia (AGA) groups were taken on different days (D_P, D_0, D_7, D_{11}, D_{15}, and D_{19}), (B): hair diameter, and (C) hair length of mice in two groups of control and with AGA on the 19th day after shaving

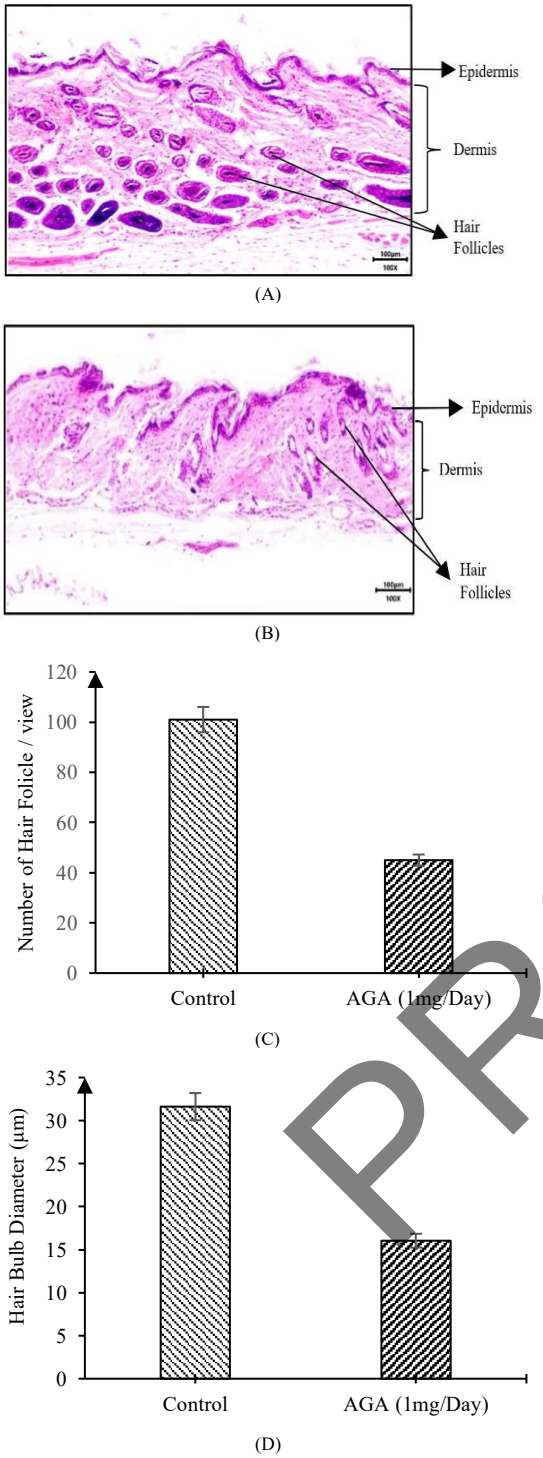

Figure 3. H&E staining image 19 days after hair shaving (Longitudinal cut): A) skin of a control mouse, B) skin of a mouse with AGA, C) The number of hair follicles in two groups of control and AGA mice, D) The diameter of hair follicles in two groups of control and AGA mice

Masson's trichrome images for the control and AGA groups are shown in Figure 4.

In the collagen of the AGA group, there is confusion compared to the control group.

Ultrasound imaging revealed that the epidermis thickness was 0.22±0.01 mm in the control group compared to 0.31±0.01 mm in the AGA group at 40 MHz. At 75 MHz, these measurements were 0.10±0.01 mm for the control group and 0.20±0.01 mm for the AGA group. The dermis thickness measurements showed 0.30±0.01 mm in the control group and 0.70±0.03 mm in the AGA group at 40 MHz, while at 75 MHz, the thicknesses were 0.40±0.02 mm for the control group and 0.70±0.03 mm for the AGA group.

3.3. Elastic Modulus Measurements (Shear Modulus and Young Modulus)

Ultrasound images taken before and after applying force in the control group and the AGA group are shown in Figure 5.

Elasticity metrics indicated a shear modulus of 1.19±0.05 kPa and 6.70±0.33 kPa for the control group and the AGA group, respectively. Young modulus demonstrated values of 6.47±0.32 kPa and 22.69±1.13 kPa for the control group and the AGA group, respectively.

The results of measuring various parameters, including hair diameter, hair length, number of hair follicles, hair bulb diameter, epidermal thickness, dermis thickness, shear modulus, and Young modulus in control and AGA groups, are shown in Table 1.

4. Discussion

This study provides significant insights into the structural alterations of skin layers in C57BL/6 mice induced by DHT to model AGA, using high-resolution ultrasound imaging. The results underscore the efficacy of ultrasound imaging as a non-invasive tool for monitoring changes in skin histology, particularly in the context of hair loss disorders such as AGA.

In this study, C57BL/6 mice were used to create an AGA model. These mice were 7 weeks old, as at this age,mice's hairs are in the telogen phase. According to the study by Fu *et al.* [6], DHT powder was injected intraperitoneally for 5 consecutive days.

To confirm the creation of the AGA disease model, photographic images were taken of the mice on the days shown in Figure 1. The results are presented in

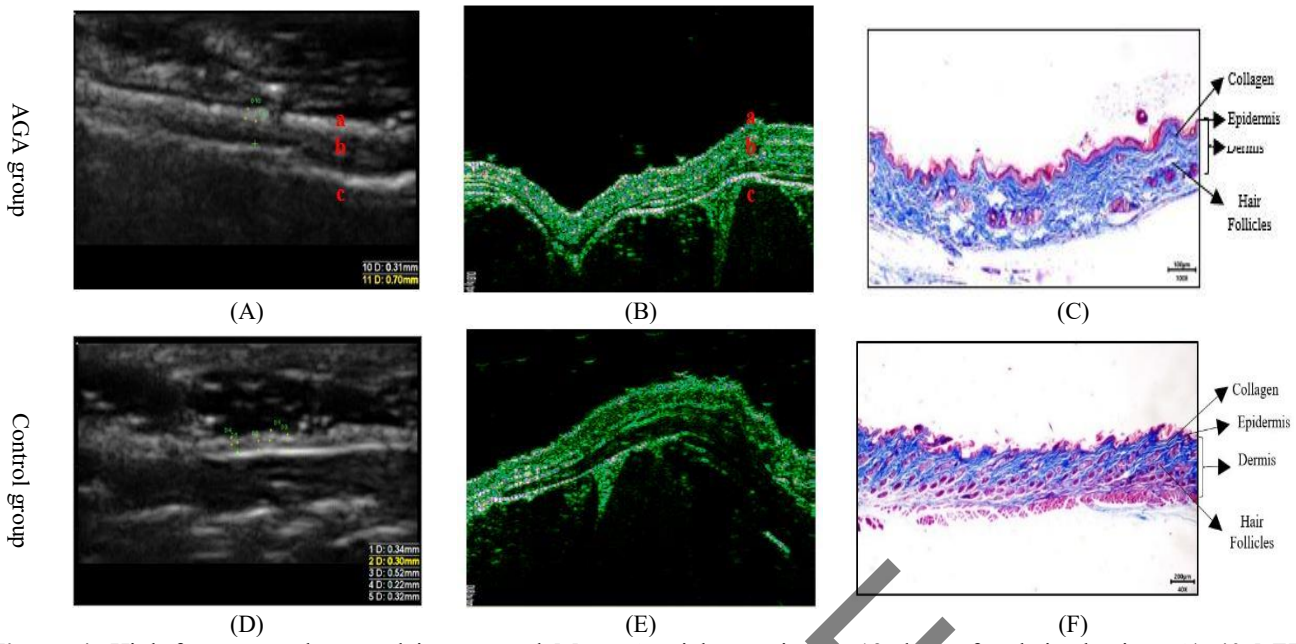

Figure 4. High-frequency ultrasound images and Masson's trichrome image 19 days after hair shaving: A) 40 MHz frequency; B) 75 MHz frequency; C) Masson's trichrome image of the skin of a mouse for AGA group; D) 40 MHz frequency; E) 75 MHz frequency probe; and F) Masson's trichrome image of the skin of a mouse for the control group

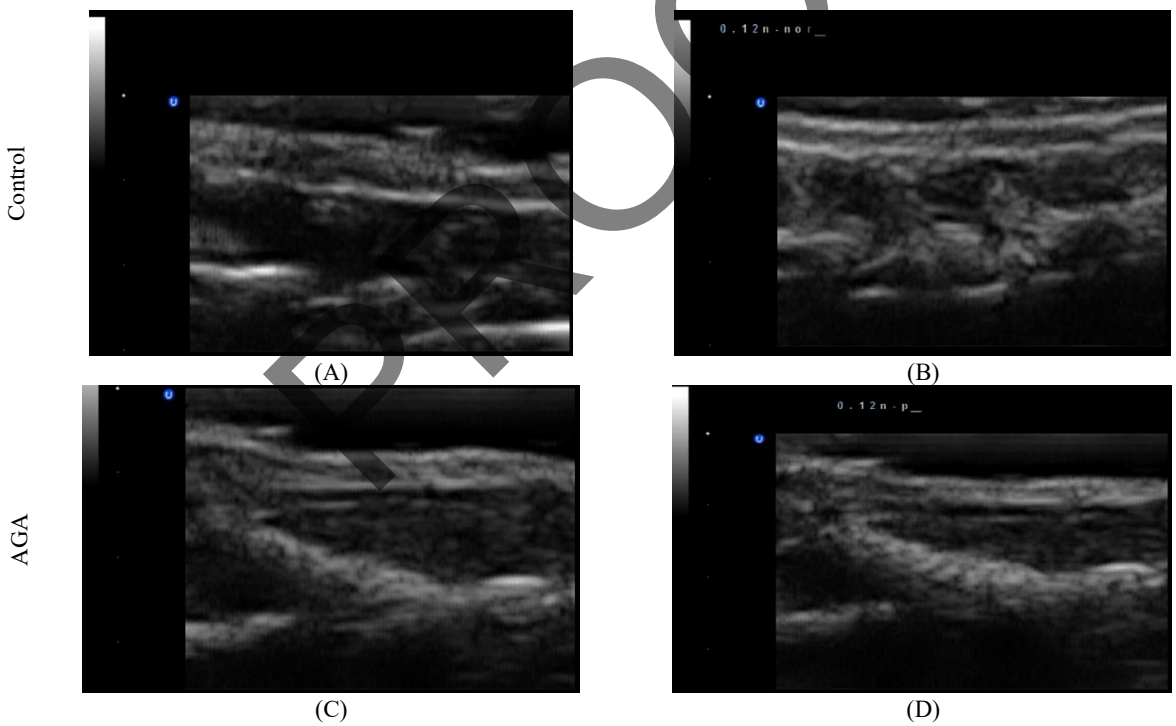

Figure 5. Ultrasound images of the skin tissue on day 19 after epilation with a 40 MHz device: (A and C) before applying stress, and (B, D) after applying stress (0.12 N) of the control and the AGA groups

Table 1. Physical and mechanical parameters were measured in the two control and Androgenetic alopecia (AGA) groups

Groups	Diameter of Hair (µm)	Length of Hair (mm)	Number of HairFollicles/view	Hair Bulb Diameter (µm)	Epidermis Thickness (mm)	Dermis Thickness (mm)	Shear Modulus (kPa)	Young Modulus (kPa)
Control	20.00±1.00	10.00±0.50	101.00±5.05	31.62±1.58	0.22±0.01	0.30±0.01	1.19±0.05	6.47±0.32
AGA	7.00±0.35	2.60±0.13	45.00±2.25	16.04±0.80	0.31±0.01	0.70±0.03	6.70±0.33	22.69±1.13
	<0.05	<0.05	<0.05	<0.05	<0.05	<0.05	<0.05	<0.05

Figure 2. As can be seen in the figure, a delay in hair growth in the mice injected with DHT, compared to the control group, is evident, which is consistent with the findings of another study [6, 25, 26]. According to Fu *et al.* [6], the maximum effect of DHT is up to 15 days after shaving the hair in mice. Therefore, hair growth may be observed in some mice injected with DHT after the 15th day. Weighing of control and AGA groups was done on the days of shaving and seven days, eleven days, fifteen days, and nineteen days after shaving, and the weight gain process was normal in both groups. Also, the length of the hair of mice injected with DHT showed less growth than the control group.

The H&E staining image of the two control and AGA groups was prepared and is shown in Figure 3. As seen in Figure 3, the number of hair follicles and the diameter of hair follicles in mice with AGA have decreased, while the diameter of the dermis and epidermis layers in these mice has increased. The amount of melanin around the hair follicles in mice with AGA showed a decrease compared to the control groups. Trichrome images were prepared for both control and AGA groups and are shown in Figure 4. In the trichrome images of the AGA group, it was observed that the collagen of the dermis layer is disordered, which is caused by the injection of DHT into this group. Based on these observations, the creation of an AGA model in mice has been confirmed.

Epidermis, dermis, and subcutaneous layers could be recognized in both images obtained from 40 MHz and 75 MHz devices in both control and AGA groups, which are shown in Figure 4. According to Figure 4, ultrasound imaging revealed that the epidermis thickness was 0.22±0.01 mm in the control group compared to 0.31±0.02 mm in the AGA group at 40 MHz. At 75 MHz, these measurements were 0.062±0.003 mm for the control group and 0.08±0.01 mm for the AGA group. The dermis thickness measurements showed 0.30±0.02 mm in the control group and 0.70±0.04 mm in the AGA group at 40 MHz, while at 75 MHz, the thicknesses were 0.65±0.03 mm for the control group and 0.70±0.04 mm for the AGA group. The data show that the administration of DHT significantly increases the thickness of both the epidermis and dermis, as evidenced by measurements taken at 40 MHz and 75 MHz ultrasound frequencies. This increase in thickness is corroborated by histological staining methods, including H&E and Masson's Trichrome, which confirm these structural changes. Such findings align with the known pathophysiological mechanisms of AGA, where DHT promotes dermal thickening and follicular miniaturization. These results are in accordance with the research findings of Fu *et al.* [6]. The results from the 40 MHz system were determined by the operator using ImageJ software to assess the area of the epidermis, dermis, and entire skin tissue. In contrast, measurements obtained from the 75 MHz system are automated.

Interestingly, the elasticity metrics reveal contrasting changes, with a remarkable reduction in both shear and Young modulus in AGA-affected skin compared to controls. These findings suggest that DHT not only increases skin layer thickness but also alters the biomechanical properties of the skin, contributing to the overall clinical picture of AGA. This diminished elasticity could be attributed to the restructuring of dermal collagen and other extracellular matrix components, which are critical determinants of skin tensile strength. While DHT may stimulate the production of collagen in response to injury or inflammation, the quality and organization of this collagen can be compromised. Collagen fibers may become disorganized or improperly aligned, which negatively impacts tensile strength and elasticity.

Naito *et al.* [27] investigated the effect of DHT injection on C57BL/6 mice. When DHT was administered to Wild-Type (WT) mice, a considerable delay in hair regrowth was observed, with it taking significantly longer to reach full regrowth compared to untreated controls. This showcases the potent inhibitory effect of DHT on hair follicles in mice that possess functioning androgen receptors. The study showed that the androgen receptor knockout) ARKO (mice, which lack functional androgen receptors had longer hair than WT mice. Specifically, the mean hair length for ARKO mice was 7.23 ± 0.51 mm, compared to 6.22 ± 0.45 mm for WT mice. This difference in hair length is likely due to the prolonged anagen phase (the active growth phase of hair) in ARKO mice, as these mice were not subjected to the inhibitory effects of DHT via androgen receptors.

Fu *et al.* [6] tested different methods of inducing AGA in C57BL/6 male mice. According to their study, the most effective method of DHT is intraperitoneal injection. They used different concentrations of DHT, and the most effective concentration was 1 mg per day for 5 days. In their study, the injection of the DHT drug into C57BL/6 mice increased the thickness of the epidermis and dermis layers. The increase in the thickness of the epidermis and dermis layers is due to inflammation. Additionally, the number of hair follicles in mice with AGA decreased. Melanin around the hair follicles is reduced in mice injected with DHT. The diameter and length of the hairs of mice under injection AGA showed a decrease compared to the healthy group. The study indicates that DHT treatment increases the expression of inflammatory cytokines such as TGF-β2, DKK1, and IL-6. These factors can contribute to fibroblast dysfunction and alter collagen synthesis, leading to weaker tissue architecture. Elevated TGF-β2, in particular, can induce fibrosis but can also lead to changes that weaken the mechanical properties of the skin due to improper collagen cross-linking.

High-resolution ultrasound, OCT, and confocal microscopy each offer unique strengths and limitations for skin imaging [14]. Ultrasound uses high-frequency sound waves to visualize deeper skin layers but provides lower resolution compared to optical methods [15]. In contrast, OCT employs near-infrared light to deliver high-axial resolution images of superficial structures, typically capturing details within the epidermis and upper dermis, albeit with limited penetration depth [13]. Confocal microscopy, meanwhile, achieves near-cellular resolution ideal for diagnosing skin anomalies non-invasively, but it is restricted to imaging only the most superficial layers. Thus, the choice among these techniques depends on the specific clinical or research requirements-whether deeper tissue evaluation or detailed surface imaging is needed [28].

The implications of these findings are particularly relevant for developing therapeutic strategies that target skin structural integrity and elasticity in AGA. The ability to non-invasively track changes in skin properties in real-time using high-resolution ultrasound could aid in the evaluation of potential treatments aimed at mitigating the effects of DHT-induced alterations. Furthermore, the study reinforces the role of the C57BL/6 mice model in understanding the complexities of AGA, which can be leveraged for testing novel pharmaceuticals or other interventions aimed at combating hair loss. It is recommended that future studies investigate the effects of different dosages of DHT on skin structure and elasticity. In future studies, we will use this model for treatment with biological factors and biostimulation. While this study provides a robust evaluation of skin changes in an AGA model, several limitations must be acknowledged. The limitations of this study are the small sample size and the lack of generalizability of the findings to other animal models and humans. Additionally, while ultrasound imaging provides detailed structural information, it does not elucidate cellular or molecular changes. Therefore, future studies should aim to integrate other imaging techniques or molecular assays to provide a more comprehensive understanding of AGA pathophysiology.

Moreover, further research should investigate the dynamic nature of these changes over time, understanding how early intervention might reverse or mitigate these structural changes. Lastly, exploring the impacts of different dosages or other androgenic compounds could provide a broader perspective on how male pattern baldness can be effectively addressed in clinical settings.

5. Conclusion

In conclusion, the study successfully harnesses high-resolution ultrasound imaging to reveal important insights into the structural and elastic changes in skin tissue associated with AGA. These findings lay a foundation for future research aimed at improving the diagnosis and treatment of hair loss conditions using advanced imaging technologies.

Acknowledgments

This study was approved by the Faculty of Medical Sciences, Tarbiat Modares University. This work was supported in part by the Iran National Science Foundation (INSF).

References

1- Ahmad Naeem and Tayyaba Anees, "DVFNet: A deep feature fusion-based model for the multiclassification of skin cancer utilizing dermoscopy images." *PloS One,* Vol. 19 (No. 3), p. e0297667, (2024).

2- Sara Yasmin Khattab, Baraa Ashraf Hijaz, and Yevgeniy Romanovich Semenov, "Cutaneous Imaging Techniques." *Hematology/Oncology Clinics,* Vol. 38 (No. 5), pp. 907-19, (2024).

3- Kate L Montgomery, Roberto A Novoa, Justin M Ko, and Gabriel N Sanchez, "Handheld multiphoton and pinhole-free reflectance confocal microscopy enables noninvasive, real-time cross-sectional imaging in skin." *Scientific Reports,* Vol. 14 (No. 1), p. 26129, (2024).

4- Bernhard Roth, Anatoly Fedorov Kukk, Di Wu, Rüdiger Panzer, and Steffen Emmert, "Four-modal device comprising optical coherence tomography, photoacoustic tomography, ultrasound, and Raman spectroscopy developed for in vivo skin lesion assessment." (2025).

5- Maria Erasti *et al.*, "Dermoscopy, Line-Field Confocal Optical Coherence Tomography, Reflectance Confocal Microscopy, and Ultra-High-Frequency Ultrasound: Clues for the Diagnosis of Hidrocystomas." *Diagnostics,* Vol. 14 (No. 23), p. 2671, (2024).

6- Zhao Feng Liu, Christopher Y Chew, Shreyas Honavar, Andrew Maxwell, Amy Sylivris, and Adam Sheridan, "Seeing beyond skin deep: high-resolution ultrasound in dermatology—a comprehensive review and future prospects." *Journal of the European Academy of Dermatology and Venereology,* Vol. 38 (No. 7), pp. 1305-13, (2024).

7- Zeinab Hormozi-Moghaddam, Manijhe Mokhtari-Dizaji, Mohammad Ali Nilforoshzade, Mohsen Bakhshande, and Sona Zare, "High-resolution ultrasound imaging for non-invasive characterization of acute wound healing in radiation injury on Guinea pig skin tissue." *Frontiers in Biomedical Technologies,* Vol. 11 (No. 1), pp. 104-12, (2024).

8- Juliana Benavides-Lara, Amanda P Siegel, Maria M Tsoukas, and Kamran Avanaki, "High-frequency photoacoustic and ultrasound imaging for skin evaluation: Pilot study for the assessment of a chemical burn." *Journal of Biophotonics,* Vol. 17 (No. 7), p. e202300460, (2024).

9- JL Perrot and E Cinotti, "High-resolution ultrasound in the current landscape of dermatology imaging." *Journal of the European Academy of Dermatology and Venereology,* Vol. 38 (No. 7), pp. 1230-31, (2024).

10- Zahra Lotfollahi, "The anatomy, physiology and function of all skin layers and the impact of ageing on the skin." *Wound Practice & Research: Journal of the Australian Wound Management Association,* Vol. 32 (No. 1), pp. 6-10, (2024).

11- Xin Tang *et al.*, "Epidermal stem cells: Skin surveillance and clinical perspective." *Journal of Translational Medicine,* Vol. 22 (No. 1), p. 779, (2024).

12- Johann Zwirner and Niels Hammer, "Anatomy and Physiology of the Skin." in *Scars: A Practical Guide for Scar Therapy*: *Springer*, (2024), pp. 3-9.

13- Nathalie Percie du Sert *et al.*, "The ARRIVE guidelines 2.0: Updated guidelines for reporting animal research." *Journal of Cerebral Blood Flow and Metabolism,* Vol. 40 (No. 9), pp. 1769-77, (2020).

14- Christelle Leon *et al.*, "Evaluation of general anesthesia protocols for a highly controlled cardiac ischemia-reperfusion model in mice." *PloS One,* Vol. 19 (No. 10), p. e0309799, (2024).

15- Mohadese Estaji, Manijhe Mokhtari-Dizaji, Mansoureh Movahedin, and Sahar Ghaffari Khaligh, "Non-invasive evaluation of elasticity of skin with the processing of ultrasound images during ultraviolet radiation: An animal photoaging model." *Photodermatology, Photoimmunology and Photomedicine,* Vol. 37 (No. 2), pp. 131-39, (2021).

16- Danlan Fu *et al.*, "Dihydrotestosterone-induced hair regrowth inhibition by activating androgen receptor in C57BL6 mice simulates androgenetic alopecia." *Biomedicine and Pharmacotherapy,* Vol. 137p. 111247, (2021).

17- Xianyan Chen *et al.*, "Dihydrotestosterone regulates hair growth through the Wnt/β-catenin pathway in C57BL/6 mice and in vitro organ culture." *Frontiers in Pharmacology,* Vol. 10p. 1528, (2020).

18- Ha-Rim Kim *et al.*, "Hair Growth Effect and the Mechanisms of Rosa rugosa Extract in DHT-Induced Alopecia Mice Model." *International Journal of Molecular Sciences,* Vol. 25 (No. 21), p. 11362, (2024).

19- A Naito *et al.*, "Dihydrotestosterone inhibits murine hair growth via the androgen receptor." *British Journal of Dermatology,* Vol. 159 (No. 2), pp. 300-05, (2008).

20- Shazli Razi *et al.*, "Line-field confocal optical coherence tomography for the diagnosis of skin tumors: a systematic review and meta-analysis." *Diagnostics,* Vol. 14 (No. 14), p. 1522, (2024).

21- J. Zwirner, N. Hammer, "Anatomy and Physiology of the Skin, in Scars: A Practical Guide for Scar Therapy". *Springer International Publishing*, pp. 3-9, (2024).

22- N. Percie du Sert, V. Hurst, A. Ahluwalia, S. Alam, M.T. Avey, M. Baker, W.J. Browne, A. Clark, I.C. Cuthill, and U. Dirnagl, "The ARRIVE Guidelines 2.0: Updated Guidelines for Reporting Animal Research". *Journal of Cerebral Blood Flow and Metabolism*, vol. 40, pp. 1769-1777, 2020.

23- C. Leon, A. Ruelle, J. Geoffray, L. Augeul, C. Vogt, P. Chiari, L. Gomez, M. Ovize, G. Bidaux, B. Pillot, "Evaluation of General Anesthesia Protocols for a Highly

Controlled Cardiac Ischemia-Reperfusion Model in Mice". *PLoS One*, vol. 19, pp. e0309799, (2024).

24- M. Estaji, M. Mokhtari-Dizaji, M. Movahedin, S. Ghaffari Khaligh, "Non-invasive Evaluation of Elasticity of Skin with the Processing of Ultrasound Images During Ultraviolet Radiation: An Animal Photoaging Model". *Photodermatology, Photoimmunology and Photomedicine*, vol. 37, pp. 131-139, (2021).

25- X. Chen, B. Liu, Y. Li, L. Han, X. Tang, W. Deng, W. Lai, M. Wan, "Dihydrotestosterone Regulates Hair Growth Through the Wnt/β-catenin Pathway in C57BL/6 Mice and In vitro Organ Culture". Frontiers in Pharmacology, vol. 10, pp. 1528, (2020).

26- H.R. Kim, J.U. Park, S.H. Lee, J.Y. Park, W. Lee, K.M. Choi, S.Y. Kim, M.H. Park, "Hair Growth Effect and the Mechanisms of Rosa rugosa Extract in DHT-Induced Alopecia Mice Model". *International Journal of Molecular Sciences*, vol. 25, pp. 11362, (2024).

27- A. Naito, T. Sato, T. Matsumoto, K. Takeyama, T. Yoshino, S. Kato, M. Ohdera, "Dihydrotestosterone Inhibits Murine Hair Growth via the Androgen Receptor". *British Journal of Dermatology*, vol. 159, pp. 300-305, (2008).

28- S. Razi, Y.H. Kuo, G. Pathak, P. Agarwal, A. Horgan, P. Parikh, F. Deshmukh, and B.K. Rao, "Line-Field Confocal Optical Coherence Tomography for the Diagnosis of Skin Tumors: A Systematic Review and Meta-Analysis". *Diagnostics*, vol. 14, pp. 1522-1533, (2024).